

Beyond leading twist: ρ meson decay constants and distribution amplitudes in a self-consistent light-front quark model

Ahmad Jafar Arifi^{1,2,*}, Ho-Meoyng Choi^{3,†} and Chueng-Ryong Ji^{4,‡}

¹*Advanced Science Research Center, Japan Atomic Energy Agency, Tokai, Ibaraki 319-1195, Japan*

²*Research Center for Nuclear Physics, The University of Osaka, Ibaraki, Osaka 567-0047, Japan*

³*Department of Physics Education, Teachers College,*

Kyungpook National University, Daegu 41566, Korea

⁴*Department of Physics, North Carolina State University, Raleigh, NC 27695-8202, USA*

(Dated: August 1, 2025)

In this study, we present a comprehensive analysis of decay constants and chiral-even and chiral-odd distribution amplitudes (DAs) up to twist 4 for the ρ meson in the standard light-front quark model (LFQM) based on the Bakamjian-Thomas (BT) construction. For the ρ meson, which possesses both longitudinal ($h = 0$) and transverse ($h = \pm 1$) polarizations, two types of decay constants, f_ρ^\parallel and f_ρ^\perp , arises accordingly. We demonstrate that these decay constants can be self-consistently extracted from both local ($z^\mu = 0$) and nonlocal ($z^\mu \neq 0$) matrix elements $\langle 0 | \bar{q}(z) \Gamma q(-z) | \rho(P, h) \rangle$, with $\Gamma = (\gamma^\mu, \sigma^{\mu\nu}, \gamma^\mu \gamma_5, \mathbf{1})$, in a manner independent of current components, polarizations, and reference frames. In particular, we emphasize the role of nonlocal matrix elements involving axial-vector and scalar currents, where mixing between f_ρ^\parallel and f_ρ^\perp occurs. We show that this mixing is consistently resolved through the BT construction, ensuring the proper extraction of these decay constants. Additionally, we investigate the structure of chiral-even DAs ($\phi_{2;V}^\parallel, \phi_{3;V}^\parallel, \psi_{3;A}^\perp, \phi_{4;V}^\parallel$) and chiral-odd DAs ($\phi_{2;T}^\perp, \phi_{3;T}^\perp, \psi_{3;S}^\parallel, \phi_{4;T}^\perp$) beyond leading twists, and present their corresponding ξ -moments and Gegenbauer moments. These results provide deeper insight into the nonperturbative structure of vector mesons and demonstrate the robustness and self-consistency of the LFQM based on the BT framework.

I. INTRODUCTION

Meson distribution amplitudes (DAs) play a fundamental role in hadron physics, encapsulating the internal quark-gluon structure of mesons and enhancing the computational precision of high-energy processes, form factors, and exclusive decays within the collinear factorization and perturbative Quantum Chromodynamics (QCD) frameworks [1–3].

As essential non-perturbative inputs, DAs provide critical insights into QCD dynamics and meson properties. Leading-twist DAs describe the momentum distribution of valence quarks, offering the primary approximation for parton distributions at high momentum. In contrast, higher-twist DAs incorporate quark-gluon interactions, transverse parton motion, and higher Fock state contributions, refining our understanding of hadronic processes across different energy scales.

The increasing experimental precision at facilities such as KEKII [4], LHC [5], JLAB [6], and the future Electron-Ion-Collider (EIC) [7, 8] presents new opportunities to explore higher-twist effects in hadronic structures [9–12]. Various theoretical approaches—including QCD sum rules (SRs) [13–19], light-cone sum rules [20], the instanton vacuum model [21–23], chiral-quark and Nambu–Jona-Lasinio models [24, 25], the Dyson-Schwinger equation (DSE) approach [26, 27], and the light-front quark

model (LFQM) [28–32]—have been employed to study leading- and higher-twist DAs.

In light-front dynamics (LFD) [33], meson DAs are defined as matrix elements of quark-antiquark bilocal operators on the light cone, providing a powerful tool for studying quark-gluon dynamics within hadrons. LFD simplifies the vacuum structure, ensures boost invariance, and facilitates factorization theorems, making it an effective framework for exploring high-energy processes and parton distributions. The LFQM, based on LFD, treats mesons as bound states of a constituent quark and a constituent antiquark and has successfully provided a unified description of meson mass spectra as well as various observables related to their wave functions [34–47]. Nevertheless, the LF zero mode remains a long-standing issue in LFD, presenting a major challenge in this framework [48–55]. While leading-twist DAs can typically be computed in a zero-mode-free manner by selecting a “good” current component, such as J^+ , the calculation of higher-twist DAs is significantly more challenging. This is because they often involve the “bad” current component, such as J^- , which requires careful treatment of LF zero modes. Therefore, accurate computations of higher-twist DAs not only serve as a crucial test of the self-consistency of phenomenological models but also provide deeper insights into hadronic quark-gluon dynamics.

In the development of the LFQM, both (1) consistency with manifest covariance and (2) a realistic phenomenological description of hadron structure and spectroscopy have been key ingredients. (1) To ensure the manifest covariance of the LFQM, one may take the approach of constructing the LFQM starting from the LF projection of a

* arifi.jafar@jaea.go.jp

† homyoung@knu.ac.kr

‡ ji@ncsu.edu

manifestly covariant Bethe-Salpeter (BS) field-theoretic model. This approach [53–56], denoted as the “LFBS model”, employs Pauli-Villars regularization to extract LF wave functions (LFWFs) and typically adopts a symmetric or non-symmetric multipole ansatz for the meson-quark vertex function. In this model, the constituent quark (Q) and antiquark (\bar{Q}) are generally off-mass-shell, leading to non-conservation of LF energy at the meson-quark vertex. This results in a nonzero binding energy, implying $M \neq M_0$, where M is the physical rest mass of the meson and M_0 is the invariant mass of the quark and antiquark. The LF zero mode arising in the LFBS model with a multipole-type wave function proportional to $1/(M^2 - M_0^2)^n$, can be explicitly identified, as discussed in Refs. [53–56]. Additionally, both potential LF zero modes and instantaneous contributions from the off-shellness of quark propagators can be carefully addressed in this framework. (2) For the more realistic phenomenology of the LFQM, the approach often referred to as “standard LFQM” has been taken, constructing the model based on a noninteracting quark-antiquark representation. This approach [34–42] employs the spin-orbit (SO) wave function obtained via the interaction-independent Melosh transformation [57], together with a Gaussian-type or other phenomenological radial wave function. In contrast to the LFBS model, the standard LFQM constrains the quark and antiquark to be on their respective mass shells, ensuring four-momentum conservation at the meson-quark vertex, $P = p_Q + p_{\bar{Q}}$, where P and $p_{Q(\bar{Q})}$ denote the momenta of the meson and its constituent quark (antiquark), respectively. Notably, conservation of LF energy ($P^- = p_{\bar{Q}}^- + p_Q^-$) at the meson-quark vertex necessitates treating the meson mass M as the invariant mass M_0 .

Our LFQM [34–39] follows the standard LFQM framework, incorporating the quark-antiquark interaction potential $V_{Q\bar{Q}}$ through a QCD-motivated effective Hamiltonian, $H_{Q\bar{Q}} = M_0 + V_{Q\bar{Q}}$. The meson mass spectrum is determined by the eigenvalue equation, $H_{Q\bar{Q}}|\Psi\rangle = (M_0 + V_{Q\bar{Q}})|\Psi\rangle$. For consistency with manifest covariance, however, this formulation aligns with the Bakamjian-Thomas (BT) construction [58, 59], in which the meson state consists of a noninteracting $Q\bar{Q}$ representation, with interactions incorporated into the mass operator, $M := M_0 + V_{Q\bar{Q}}$. This approach ensures the preservation of the Poincaré group structure and commutation relations.

While standard LFQMs generally offer greater predictive power than LFBS models, their lack of manifest covariance complicates the treatment of LF zero modes. Hadronic matrix elements are typically computed as

$$\langle P' | \bar{q} \Gamma^\mu q | P \rangle = \mathcal{P}^\mu \mathcal{F}, \quad (1)$$

where \mathcal{F} represents an observable (e.g, decay constants or form factors), and \mathcal{P}^μ is the associated Lorentz factor.

In most standard LFQM calculations of Eq. (1), referred to as the “conventional LFQM”, the BT construction ($M \rightarrow M_0$) is applied only to the matrix element, while \mathcal{P}^μ is treated as an external kinematic variable,

independent of internal momenta:

$$\mathcal{F} = \frac{1}{\mathcal{P}^\mu} \langle P' | \bar{q} \Gamma^\mu q | P \rangle_{\text{BT}}. \quad (2)$$

The subscript “BT” highlights that the BT construction is applied only to the matrix element, but not to the Lorentz factor \mathcal{P}^μ . It is often observed from Eq. (2) that when \mathcal{F} is extracted from a “good” current component, such as the plus current, where \mathcal{P}^+ is independent of M , it remains free from LF zero modes. However, when computed from the minus current, where \mathcal{P}^- explicitly depends on M , \mathcal{F} generally exhibits LF zero modes.

In our recent studies on the decay constants of pseudoscalar and vector mesons [39, 60] and the pion electromagnetic form factor [61] within the standard LFQM, we explicitly demonstrated that ensuring current-component independence in \mathcal{F} requires the uniform application of the BT construction. Specifically, the substitution $M \rightarrow M_0$ must be applied consistently to both the matrix element and the Lorentz factor. This formulation guarantees self-consistency and eliminates LF zero mode contamination by computing

$$\mathcal{F} = \langle P' | \frac{\bar{q} \Gamma^\mu q}{\mathcal{P}^\mu} | P \rangle_{\text{BT}}, \quad (3)$$

where the subscript “BT” indicates that \mathcal{P}^μ is evaluated within the integral over internal momenta. In particular, for the minus current, the physical mass M in \mathcal{P}^- must be replaced with M_0 . This substitution effectively absorbs the LF zero mode, ensuring a well-defined and physically meaningful formalism.

The uniform application of the BT construction in the standard LFQM, as demonstrated in Refs. [46, 60, 61], was first proposed in Ref. [30] for vector meson decay constants. This approach originates from the covariant BS model [54, 55] and transitions to the standard LFQM via a matching condition, which we termed the “Type II” link (see Eq. (49) in Ref. [30]). A key aspect of this link is replacing M in matrix element integrands with M_0 , effectively imposing the on-mass-shell condition for the constituent quark and antiquark in the LFQM.

Subsequent studies utilizing this link have explored twist-2 and twist-3 DAs and decay constants for pseudoscalar mesons [31, 32], as well as semileptonic and rare decays between pseudoscalar mesons [43, 44], consistently yielding current-component-independent results. Notably, in Ref. [39], the equivalence between results obtained via the Type II link and direct LFQM calculations was explicitly demonstrated, further validating its role in ensuring self-consistency across analyses. To highlight this systematic approach—aligned with the BT construction in computing physical observables—we refer to our framework as the “self-consistent LFQM”.

The purpose of this work is to complete the study of vector meson properties by extending our previous self-consistent LFQM analyses [30, 39] on vector meson decay constants and chiral-even DAs to include chiral-odd DAs up to twist 4.

For the ρ meson, which has both longitudinal ($h = 0$) and transverse ($h = \pm 1$) polarizations, there exist two types of decay constants: f_ρ^\parallel and f_ρ^\perp , respectively. We demonstrate that these decay constants, associated with polarization vectors ϵ_h , can be consistently obtained from the matrix elements $\langle 0 | \bar{q}(z) \Gamma q(-z) | \rho(P, h) \rangle$, where $\Gamma = (\gamma^\mu, \sigma^{\mu\nu}, \gamma^\mu \gamma_5, \mathbf{1})$ for both local ($z^\mu = 0$) and nonlocal ($z^\mu \neq 0$) matrix elements, in a process-independent manner. Of particular importance are the nonlocal matrix elements involving axial-vector and scalar currents, where mixing occurs between f_ρ^\parallel and f_ρ^\perp . We show that the correct extraction of these decay constants from the mixing is ensured by employing the BT construction.

Furthermore, we examine the structure of chiral-even DAs ($\phi_{2;V}^\parallel, \phi_{3;V}^\parallel, \psi_{3;A}^\perp, \phi_{4;V}^\parallel$) and chiral-odd DAs ($\phi_{2;T}^\perp, \phi_{3;T}^\perp, \psi_{3;S}^\parallel, \phi_{4;T}^\perp$) beyond leading twist, along with their ξ -moments and Gegenbauer moments. Their behavior in the chiral limit ($m \rightarrow 0$) is also computed, showing consistency with results from QCD sum rules [13].

The paper is organized as follows: In Sec. II, we outline the LFQM and describe the light-front wave functions of the $\rho(1S)$ meson. Section III examines the decay constants derived from four distinct current operators, demonstrating their process independence and rotational invariance. In Sec. IV, we discuss chiral-even and chiral-odd DAs up to twist 4, obtained from three local and nonlocal current operators Γ , and analyze their ξ -moments and Gegenbauer moments. Finally, Section V presents our conclusions.

II. LIGHT-FRONT QUARK MODEL

In our LFQM [34–39], a meson is described as a quark-antiquark bound state with total momentum P , where the Fock state expansion is truncated to include only the constituent quark (Q) and antiquark (\bar{Q}). The model represents the Fock state as a noninteracting $Q\bar{Q}$ pair, with their interactions incorporated into the mass operator, defined as $M := M_0 + V_{Q\bar{Q}}$. This formulation ensures consistency with the Poincaré group’s commutation relations for a two-body bound state. The resulting interactions are encapsulated in the LFWF $\Psi_{Q\bar{Q}}$, which is obtained as the eigenfunction of the QCD-motivated effective Hamiltonian: $H_{Q\bar{Q}} | \Psi_{Q\bar{Q}} \rangle = M | \Psi_{Q\bar{Q}} \rangle$ [34–39].

In our LFQM mass spectrum analysis, a Gaussian-type radial wave function [34, 35] is used as a variational trial function to determine mass eigenvalues and model parameters. Other types of radial wave functions, such as power-law [28], harmonic oscillator (HO) [36–38, 62], or Gaussian expansion [45], have also been employed to model the wave functions and improve specific features. Once these parameters are fixed, they are applied to compute observables such as decay constants and form factors [29, 34–38, 43]. Focusing on the self-consistent analysis of decay constants and higher-twist DAs for the $\rho(1S)$ meson, we provide a brief overview of the LFWFs,

highlighting key aspects constrained by the on-mass-shell condition of its constituents.

The meson’s four-momentum in LFD is given by $P = (P^+, P^-, \mathbf{P}_\perp)$, where $P^+ = P^0 + P^3$ and $P^- = P^0 - P^3$ denote the LF longitudinal momentum and energy, respectively, while $\mathbf{P}_\perp = (P^1, P^2)$ represents the transverse momenta. We adopt the metric convention $P^2 = P^+ P^- - \mathbf{P}_\perp^2$.

The meson state $|\mathcal{M}(P, J, h)\rangle$, with momentum P and spin state (J, h) , is constructed as [40, 63, 64]

$$|\mathcal{M}\rangle = \int [d^3\bar{p}_1] [d^3\bar{p}_2] 2(2\pi)^3 \delta^3(\bar{P} - \bar{p}_1 - \bar{p}_2) \times \sum_{\lambda_1, \lambda_2} \Psi_{\lambda_1 \lambda_2}^{Jh}(x, \mathbf{k}_\perp) |q_{\lambda_1}(p_1) \bar{q}_{\lambda_2}(p_2)\rangle, \quad (4)$$

where p_i^μ and λ_i are the on-mass-shell ($p_i^2 = m_i^2$) momenta and helicities of the constituent quark ($i = 1$) and antiquark ($i = 2$), respectively. The LF three-momentum is defined as $\bar{p} = (p^+, \mathbf{p}_\perp)$, with the integration measure $[d^3\bar{p}] \equiv dp^+ d^2\mathbf{p}_\perp / (16\pi^3)$. The LF internal relative momentum variables (x, \mathbf{k}_\perp) are defined as $x_i = p_i^+ / P^+$ and $\mathbf{k}_{i\perp} = \mathbf{p}_{i\perp} - x_i \mathbf{P}_\perp$, where $\sum_i x_i = 1$ and $\sum_i \mathbf{k}_{i\perp} = 0$. We set $x = x_1$ and $\mathbf{k}_\perp = \mathbf{k}_{1\perp}$. The meson state satisfies the normalization condition:

$$\langle \mathcal{M}' | \mathcal{M} \rangle = 2(2\pi)^3 P^+ \delta^3(\bar{P}' - \bar{P}) \delta_{J'J} \delta_{h'h}, \quad (5)$$

where $\mathcal{M}' = \mathcal{M}(P', J', h')$.

In momentum space, the LFWF of a meson is decomposed as

$$\Psi_{\lambda_1 \lambda_2}^{Jh}(x, \mathbf{k}_\perp) = \Phi(x, \mathbf{k}_\perp) \mathcal{R}_{\lambda_1 \lambda_2}^{Jh}(x, \mathbf{k}_\perp), \quad (6)$$

where $\Phi(x, \mathbf{k}_\perp)$ is the radial wave function used in our variational mass spectroscopic analysis [34–38], and $\mathcal{R}_{\lambda_1 \lambda_2}^{Jh}$ is the spin-orbit (SO) wave function, obtained via the interaction-independent Melosh transformation [57], from the ordinary SO wave function assigned by the quantum number J^{PC} .

A key feature of the LF formulation for bound states, as expressed in Eq. (4), is the frame independence of the LFWF [33]. Unlike in the instant form, where wave functions depend on the hadron’s overall motion, the internal variables (x, \mathbf{k}_\perp) in the LFWF remain unchanged under boosts to any physical (P^+, \mathbf{P}_\perp) frame.

In our LFQM, the ρ meson is treated under SU(2) isospin symmetry, assuming equal up and down quark masses, denoted as $m_1 = m_2 = m$. The interaction-independent SO wave function, consistent with the BT construction, can then be written in a covariant form [41, 42] as

$$\mathcal{R}_{\lambda_1 \lambda_2}^{1h} = \frac{1}{\sqrt{2}M_0} \bar{u}_{\lambda_1}(p_1) \left[-\not{\epsilon}_h + \frac{(p_1 - p_2) \cdot \epsilon_h}{M_0 + 2m} \right] v_{\lambda_2}(p_2), \quad (7)$$

where the boost-invariant meson mass squared is given by

$$M_0^2 = \frac{\mathbf{k}_\perp^2 + m^2}{x(1-x)}. \quad (8)$$

In this LFQM framework, based on the BT construction, the polarization vectors ϵ_h^μ ($h = \pm 1, 0$) satisfy the transversality condition $\epsilon \cdot P = 0$, where $P^- = \frac{M_0^2 + \mathbf{P}_\perp^2}{P^+}$ ensures the LF energy conservation, i.e., $P^- = p_{\bar{Q}}^- + p_Q^-$, at the meson-quark vertex. Consequently, the polarization vectors are expressed in terms of M_0 as [41, 42]

$$\begin{aligned} \epsilon_\pm^\mu &= \left(0, \frac{2}{P^+} \epsilon_\perp(\pm) \cdot \mathbf{P}_\perp, \epsilon_\perp(\pm) \right), \\ \epsilon_0^\mu &= \frac{1}{M_0} \left(P^+, \frac{\mathbf{P}_\perp^2 - M_0^2}{P^+}, \mathbf{P}_\perp \right), \end{aligned} \quad (9)$$

where $\epsilon_\perp(\pm) = \mp \frac{1}{\sqrt{2}}(1, \pm i)$.

Using Dirac helicity spinors [1, 41] along with the polarization vectors above, the explicit matrix forms of the SO wave functions for the vector meson are given by

$$\begin{aligned} \mathcal{R}_{\lambda_1 \lambda_2}^{1+1}(x, \mathbf{k}_\perp) &= \mathcal{R}_0 \begin{pmatrix} m + \frac{\mathbf{k}_\perp^2}{M_0 + 2m} & k_\perp^{(+)} \frac{\mathcal{M}_1}{M_0 + 2m} \\ -k_\perp^{(+)} \frac{\mathcal{M}_2}{M_0 + 2m} & -\frac{(k_\perp^{(+)})^2}{M_0 + 2m} \end{pmatrix}, \\ \mathcal{R}_{\lambda_1 \lambda_2}^{10}(x, \mathbf{k}_\perp) &= \frac{\mathcal{R}_0}{\sqrt{2}} \begin{pmatrix} k_\perp^{(-)} \frac{\mathcal{M}_2 - \mathcal{M}_1}{M_0 + 2m} & m + \frac{2\mathbf{k}_\perp^2}{M_0 + 2m} \\ m + \frac{2\mathbf{k}_\perp^2}{M_0 + 2m} & -k_\perp^{(+)} \frac{\mathcal{M}_2 - \mathcal{M}_1}{M_0 + 2m} \end{pmatrix}, \\ \mathcal{R}_{\lambda_1 \lambda_2}^{1-1}(x, \mathbf{k}_\perp) &= \mathcal{R}_0 \begin{pmatrix} -\frac{(k_\perp^{(-)})^2}{M_0 + 2m} & k_\perp^{(-)} \frac{\mathcal{M}_2}{M_0 + 2m} \\ -k_\perp^{(-)} \frac{\mathcal{M}_1}{M_0 + 2m} & m + \frac{\mathbf{k}_\perp^2}{M_0 + 2m} \end{pmatrix}, \end{aligned} \quad (10)$$

where $k_\perp^{(\pm)} = k_x \pm ik_y$, $\mathcal{R}_0 = 1/\sqrt{m^2 + \mathbf{k}_\perp^2}$, and $\mathcal{M} = \mathcal{M}_2 - \mathcal{M}_1$ with $\mathcal{M}_1 = xM_0 + m$ and $\mathcal{M}_2 = (1-x)M_0 + m$. We note that $\mathcal{R}_{\lambda_1 \lambda_2}^{Jh}$ satisfy the orthogonality condition $\sum_{\lambda_1, \lambda_2} \mathcal{R}_{\lambda_1 \lambda_2}^{Jh\dagger} \mathcal{R}_{\lambda_1 \lambda_2}^{J'h'} = \delta_{JJ'} \delta_{hh'}$.

For the radial wave function, we adopt the following rotationally invariant Gaussian form:

$$\Phi(\mathbf{k}) = \frac{4\pi^{3/4}}{\beta^{3/2}} e^{-\mathbf{k}^2/2\beta^2}, \quad (11)$$

where $\mathbf{k} = (k_z, \mathbf{k}_\perp)$, and β serves as a variational parameter in our mass spectroscopic analysis [34–38]. The Gaussian wave function satisfies the normalization condition

$$\int \frac{d^3\mathbf{k}}{2(2\pi)^3} |\Phi(\mathbf{k})|^2 = 1. \quad (12)$$

To ensure rotational invariance, we express the normalization of $\Phi(\mathbf{k})$ in terms of $\Phi(x, \mathbf{k}_\perp)$ by transforming variables $(k_z, \mathbf{k}_\perp) \rightarrow (x, \mathbf{k}_\perp)$:

$$\int_0^1 dx \int \frac{d^2\mathbf{k}_\perp}{2(2\pi)^3} |\Phi(x, \mathbf{k}_\perp)|^2 = 1. \quad (13)$$

The wave function $\Phi(x, \mathbf{k}_\perp)$ includes the Jacobian factor:

$$\Phi(x, \mathbf{k}_\perp) = \sqrt{\frac{\partial k_z}{\partial x}} \Phi(\mathbf{k}), \quad (14)$$

where $k_z = \frac{1}{2}(2x-1)M_0$ and $\frac{\partial k_z}{\partial x} = \frac{M_0}{4x(1-x)}$ for the case of equal quark and antiquark masses.

The total LFWF, given by Eq. (6), satisfies the same normalization condition as Eq. (13). This follows from the meson state $|\mathcal{M}(P, J, h)\rangle$ obeying the normalization in Eq. (5), and the SO wave function being the unitary. In particular, the inclusion of the Jacobian factor in $\Phi(x, \mathbf{k}_\perp)$ ensures the rotational invariance of the model wave function, yielding self-consistent results that are independent of current components and invariant under boosts.

III. DECAY CONSTANTS

In this section, we begin by reviewing the calculation of decay constants derived from local matrix elements of the vector and tensor current operators, using various current components and polarization vectors [39], as summarized in Table I. We then provide a detailed analysis of decay constants obtained from nonlocal matrix elements involving axial-vector and scalar current operators, which is the main focus of this work. Particular emphasis is placed on achieving self-consistency within the model, based on the BT construction [30–32, 39, 43].

A. Vector and Tensor Currents

The decay constants f_ρ^\parallel and f_ρ^\perp , corresponding to the longitudinally and transversely polarized ρ meson, are defined via the local matrix elements of the vector ($\Gamma_V^\mu \equiv \gamma^\mu$) and tensor ($\Gamma_T^{\mu\nu} \equiv \sigma^{\mu\nu}$) current operators [13]

$$\begin{aligned} \langle 0 | \bar{q}(0) \Gamma_V^\mu q(0) | \rho(P, h) \rangle &= f_\rho^\parallel \mathcal{P}_V^\mu, \\ \langle 0 | \bar{q}(0) \Gamma_T^{\mu\nu} q(0) | \rho(P, h) \rangle &= f_\rho^\perp \mathcal{P}_T^{\mu\nu}, \end{aligned} \quad (15)$$

where $\mathcal{P}_V^\mu = M \epsilon_h^\mu$ and $\mathcal{P}_T^{\mu\nu} = i(\epsilon_h^\mu P^\nu - \epsilon_h^\nu P^\mu)$. Here, M and ϵ_h^μ denote the mass and polarization vector of the ρ meson.

In the standard LFQM, the decay amplitudes for the current operators $\Gamma = \Gamma_V^\mu$ or $\Gamma = \Gamma_T^{\mu\nu}$ are given by

$$\begin{aligned} \langle 0 | \bar{q} \Gamma q | \rho(P, h) \rangle &= \sqrt{N_c} \int_0^1 dx \int \frac{d^2\mathbf{k}_\perp}{16\pi^3} \Phi(x, \mathbf{k}_\perp) \\ &\times \sum_{\lambda_1, \lambda_2} \mathcal{R}_{\lambda_1 \lambda_2}^{1h} \left[\frac{\bar{v}_{\lambda_2}(p_2)}{\sqrt{x_2}} \Gamma \frac{u_{\lambda_1}(p_1)}{\sqrt{x_1}} \right], \end{aligned} \quad (16)$$

where the color factor $N_c = 3$ arises from the implicit color structure of the wave function [40, 42].

In the LFQM analysis [39], formulated within the BT construction ($M \rightarrow M_0$), we explicitly demonstrated that f_ρ^\parallel and f_ρ^\perp can be obtained in a way that is independent of current components, polarization vectors, and reference frames, by computing

$$\begin{aligned} f_\rho^\parallel &= \langle 0 | \frac{\bar{q} \gamma^\mu q}{\mathcal{P}_V^\mu} | P \rangle_{\text{BT}}, \\ f_\rho^\perp &= \langle 0 | \frac{\bar{q} \sigma^{\mu\nu} q}{\mathcal{P}_T^{\mu\nu}} | P \rangle_{\text{BT}}. \end{aligned} \quad (17)$$

TABLE I. Operators $\mathcal{O}_{V(T)}$ from Eq. (20) for all possible components of the currents Γ_V^μ ($\Gamma_T^{\mu\nu}$) and the polarization vectors ϵ_h [39].

	$\Gamma_V = \gamma^\mu$	ϵ_h	$\mathcal{O}_V^\mu(h)$
	γ^+, γ^\perp	ϵ_0	$\sqrt{2}\mathcal{R}_0 \left(2m + \frac{4\mathbf{k}_\perp^2}{M_0+2m}\right)$
f_ρ^\parallel	γ^-	ϵ_0	$\sqrt{2}\mathcal{R}_0 \left(2m + \frac{4\mathbf{k}_\perp^2}{M_0+2m}\right)$
	γ^\perp, γ^-	ϵ_+	$\sqrt{2}\mathcal{R}_0 \left(M_0 - \frac{2\mathbf{k}_\perp^2}{M_0+2m}\right)$
	$\Gamma_T = \sigma^{\mu\nu}$	ϵ_h	$\mathcal{O}_T^{\mu\nu}(h)$
	$\sigma^{\perp+}, \sigma^{+-}$	ϵ_+	$\sqrt{2}\mathcal{R}_0 \left(2m + \frac{2\mathbf{k}_\perp^2}{M_0+2m}\right)$
f_ρ^\perp	$\sigma^{\perp-}$	ϵ_+	$\sqrt{2}\mathcal{R}_0 \left(2m + \frac{2\mathbf{k}_\perp^2}{M_0+2m}\right)$
	$\sigma^{+-}, \sigma^{\perp-}$	ϵ_0	$\sqrt{2}\mathcal{R}_0 \left(M_0 - \frac{4\mathbf{k}_\perp^2}{M_0+2m}\right)$

Here, the physical mass M included in Lorentz factors \mathcal{P}_V^μ and $\mathcal{P}_T^{\mu\nu}$ is replaced with the invariant mass M_0 , and the Lorentz factors are evaluated within the integral over internal momenta.

The decay constants $f_\rho^{\parallel(\perp)}$, defined in Eq. (17), can be expressed in a generic integral form as

$$f_\rho^{\parallel(\perp)} = \sqrt{N_c} \int_0^1 dx \int \frac{d^2\mathbf{k}_\perp}{16\pi^3} \Phi(x, \mathbf{k}_\perp) \times \frac{1}{\mathcal{P}_{V(T)}} \sum_{\lambda_1, \lambda_2} \mathcal{R}_{\lambda_1 \lambda_2}^{1h} \left[\frac{\bar{v}_{\lambda_2}(p_2)}{\sqrt{x_2}} \Gamma_{V(T)} \frac{u_{\lambda_1}(p_1)}{\sqrt{x_1}} \right]. \quad (18)$$

For simplicity, we omit the explicit Lorentz indices of $(\mathcal{P}_V^\mu, \Gamma_V^\mu)$ and $(\mathcal{P}_T^{\mu\nu}, \Gamma_T^{\mu\nu})$, although they are implicitly carried through the calculations for various current components and polarization vectors.

While the explicit forms of $f_\rho^{\parallel(\perp)}$ for all current components and polarization vectors were provided in Ref. [39], we summarize the final compact expressions here for completeness:

$$f_\rho^{\parallel(\perp)} = \sqrt{N_c} \int_0^1 dx \int \frac{d^2\mathbf{k}_\perp}{16\pi^3} \Phi(x, \mathbf{k}_\perp) \mathcal{O}_{V(T)}, \quad (19)$$

where the operators $\mathcal{O}_{V(T)}$ are defined as

$$\mathcal{O}_{V(T)} = \frac{1}{\mathcal{P}_{V(T)}} \sum_{\lambda_1, \lambda_2} \mathcal{R}_{\lambda_1 \lambda_2}^{1h} \left[\frac{\bar{v}_{\lambda_2}(p_2)}{\sqrt{x_2}} \Gamma_{V(T)} \frac{u_{\lambda_1}(p_1)}{\sqrt{x_1}} \right]. \quad (20)$$

These operators are derived using the Dirac helicity spinors [1, 41] and the SO wave functions defined in Eq. (10).

The complete results for $f_\rho^{\parallel(\perp)}$ with all current components and polarization vectors are summarized in Table I. Notably, the expressions for f_ρ^\parallel obtained from ϵ_0 with any current γ^μ are identical in functional form. Although the results derived using ϵ_+ with (γ^\perp, γ^-) differ in form from those with ϵ_0 , they yield the same numerical values. This demonstrates the current-component independence of our formalism, with a similar pattern observed for f_ρ^\perp . This independence is achieved through the incorporation of the Lorentz structures $\mathcal{P}_{V(T)}$ inside the integral and the consistent replacement of M with M_0 . These features ensure that the decay constants are independent of current components and polarization vectors, maintain boost invariance, and remain self-consistent within the model framework—a key hallmark of our LFQM based on the BT construction [30–32, 39, 43].

B. Axial-Vector and Scalar Currents

The main focus of this work is the calculation of non-local matrix elements of the axial-vector ($\Gamma_A^\mu = \gamma^\mu \gamma_5$) and scalar ($\Gamma_S = \mathbf{1}$) current operators, further extending our LFQM framework based on the BT construction [30–32, 39, 43].

The decay constants of the ρ meson can be extracted from these nonlocal matrix elements, defined in Ref. [13], as

$$\begin{aligned} A_A^\mu &= \langle 0 | \bar{q}(z) \gamma^\mu \gamma^5 [z, -z] q(-z) | \rho(P, h) \rangle \\ &= f_\rho^A \mathcal{P}_A^\mu \int_0^1 dx e^{i\zeta P \cdot z} \psi_{3;A}^\perp(x), \\ A_S &= \langle 0 | \bar{q}(z) \mathbf{1} [z, -z] q(-z) | \rho(P, h) \rangle \\ &= -i f_\rho^S \mathcal{P}_S \int_0^1 dx e^{i\zeta P \cdot z} \psi_{3;S}^\parallel(x), \end{aligned} \quad (21)$$

where $\mathcal{P}_A^\mu = \frac{1}{2} M \epsilon_{\nu\alpha\beta}^\mu \epsilon_h^\nu P^\alpha z^\beta$, $\mathcal{P}_S = M^2 (\epsilon_h \cdot z)$, and $\zeta = 2x - 1$. The constants f_ρ^A and f_ρ^S are the decay constants associated with the axial-vector and scalar currents, respectively. The two-particle twist-3 DAs, $\psi_{3;A}^\perp(x)$ and $\psi_{3;S}^\parallel(x)$, satisfy the normalization condition

$$\int_0^1 dx \psi_{3;A(S)}^{\perp(\parallel)}(x) = 1. \quad (22)$$

The path-ordered gauge factor $[z, -z]$, ensuring gauge invariance, is set to unity in the LF gauge ($A^+ = 0$) throughout this work. Since f_ρ^A and f_ρ^S are defined through these nonlocal matrix elements, their extraction requires working in the nonlocal LF limit, with $z^+ = z_\perp = 0$. Thus, determining $\psi_{3;A}^\perp(x)$ and $\psi_{3;S}^\parallel(x)$ is essential to obtain these decay constants.

We first present the calculation of $\psi_{3;S}^\parallel(x)$ and f_ρ^S by integrating both sides of Eq. (21) with respect to z^- ,

using the dummy variable x' (and $\zeta' = 2x' - 1$), as follows:

$$\begin{aligned} & \int_{-\infty}^{\infty} \frac{dz^-}{2\pi} e^{-i\zeta' P \cdot z} \langle 0 | \bar{q}(z) q(-z) | \rho(P, h) \rangle \\ &= C_S \int_0^1 dx \int_{-\infty}^{\infty} \frac{dz^-}{2\pi} z^- e^{-i(x'-x)P^+ z^-} \psi_{3;S}^{\parallel}(x), \end{aligned} \quad (23)$$

where $C_S = -\frac{i}{2} f_{\rho}^S M^2 \epsilon_h^+$. It is important to note that only the longitudinal ($h = 0$) polarization vector contributes to the extraction of f_{ρ}^S .

The integration of the right-hand side (RHS) of Eq. (23) over z^- is given by [60]

$$\begin{aligned} & \int_{-\infty}^{\infty} \frac{dz^-}{2\pi} z^- e^{-i(x'-x)P^+ z^-} \psi_{3;S}^{\parallel}(x) \\ &= \frac{i}{(P^+)^2} \frac{\partial}{\partial x'} \left[\delta(x - x') \psi_{3;S}^{\parallel}(x) \right]. \end{aligned} \quad (24)$$

This leads to

$$\text{RHS of Eq. (23)} = \frac{f_{\rho}^S M^2 \epsilon_0^+}{2(P^+)^2} \frac{\partial \psi_{3;S}^{\parallel}(x')}{\partial x'}. \quad (25)$$

The left-hand side (LHS) of Eq. (23) can be written in our LFQM as

$$\begin{aligned} & \text{LHS of Eq. (23)} \\ &= \sqrt{N_c} \int_0^1 dx \int \frac{d^2 \mathbf{k}_{\perp}}{16\pi^3} \int_{-\infty}^{\infty} \frac{dz^-}{2\pi} e^{-i\zeta' P \cdot z} e^{-i(p_2 - p_1) \cdot z} \\ & \times \sum_{\lambda_1, \lambda_2} \Psi_{\lambda_1 \lambda_2}^{10}(x, \mathbf{k}_{\perp}) \left[\frac{\bar{v}_{\lambda_2}(p_2) u_{\lambda_1}(p_1)}{\sqrt{x'_2} \sqrt{x'_1}} \right], \end{aligned} \quad (26)$$

where $\Psi_{\lambda_1 \lambda_2}^{10}(x, \mathbf{k}_{\perp})$ is the LFWF defined in Eq. (6). Since $e^{-i\zeta' P \cdot z} e^{-i(p_2 - p_1) \cdot z} = e^{-i(x'-x)P^+ z^-}$, the z^- integration yields $\delta[(x'-x)P^+]$. Substituting this result leads to

$$\begin{aligned} & \text{LHS of Eq. (23)} \\ &= \frac{\sqrt{N_c}}{P^+} \int \frac{d^2 \mathbf{k}_{\perp}}{16\pi^3} \sum_{\lambda_1, \lambda_2} \Psi_{\lambda_1 \lambda_2}^{10}(x', \mathbf{k}_{\perp}) \left[\frac{\bar{v}_{\lambda_2}(p'_2) u_{\lambda_1}(p'_1)}{\sqrt{x'_2} \sqrt{x'_1}} \right], \end{aligned} \quad (27)$$

where the prime ($'$) in $\Psi_{\lambda_1 \lambda_2}^{10}(x', \mathbf{k}_{\perp})$ and in p_i indicates that the longitudinal momentum fractions inside the integral are expressed in terms of x' , specifically, $x'_1 = x'$ and $x'_2 = 1 - x'$.

By integrating both Eqs. (25) and (27) over x' , we obtain

$$\begin{aligned} \psi_{3;S}^{\parallel}(x) &= \frac{\sqrt{N_c}}{f_{\rho}^S} \int_0^1 dx' \int \frac{d^2 \mathbf{k}_{\perp}}{16\pi^3} \Phi(x', \mathbf{k}_{\perp}) \\ & \times \frac{2P^+}{M^2 \epsilon_0^+} \sum_{\lambda_1, \lambda_2} \mathcal{R}'_{\lambda_1 \lambda_2}{}^{10} \left[\frac{\bar{v}_{\lambda_2}(p'_2) u_{\lambda_1}(p'_1)}{\sqrt{x'_2} \sqrt{x'_1}} \right]. \end{aligned} \quad (28)$$

By integrating both sides over x and applying the normalization condition given in Eq. (22), the decay constant f_{ρ}^S is given by

$$\begin{aligned} f_{\rho}^S &= \sqrt{N_c} \int_0^1 dx \int_0^x dx' \int \frac{d^2 \mathbf{k}_{\perp}}{16\pi^3} \Phi(x', \mathbf{k}_{\perp}) \\ & \times \frac{2P^+}{M^2 \epsilon_0^+} \sum_{\lambda_1, \lambda_2} \mathcal{R}'_{\lambda_1 \lambda_2}{}^{10} \left[\frac{\bar{v}_{\lambda_2}(p'_2) u_{\lambda_1}(p'_1)}{\sqrt{x'_2} \sqrt{x'_1}} \right]. \end{aligned} \quad (29)$$

In our LFQM based on the BT construction, we replace the physical mass M with the invariant mass M_0 in the integrand, i.e., $\frac{P^+}{M^2 \epsilon_0^+} \rightarrow \frac{1}{M_0}$, to obtain f_{ρ}^S . This yields the final expression:

$$f_{\rho}^S = \sqrt{N_c} \int_0^1 dx \int_0^x dx' \int \frac{d^2 \mathbf{k}_{\perp}}{16\pi^3} \Phi(x', \mathbf{k}_{\perp}) \mathcal{O}'_S, \quad (30)$$

where

$$\mathcal{O}'_S = 2\sqrt{2} \mathcal{R}_0(1 - 2x') M'_0. \quad (31)$$

The resulting numerical value of f_{ρ}^S is then substituted back into Eq. (28), applying the same replacement to determine $\psi_{3;S}^{\parallel}(x)$.

Now, for the computation of $\psi_{3;A}^{\perp}(x)$ and f_{ρ}^A in Eq. (21), the only nonvanishing Lorentz factor is $\mathcal{P}_A^{\mu} = \frac{1}{2} M \epsilon_{\nu\alpha}^{\mu} \epsilon_{\pm}^{\nu} p^{\alpha} z^{-}$. This implies that only the transverse ($h = \pm$) polarization vectors contribute. Furthermore, in the $\mathbf{P}_{\perp} = 0$ frame, only \mathcal{P}_A^{\perp} remains nonzero. For instance¹, for $\mu = x$, $\epsilon_{y+-}^x \epsilon_{+}^y p^+ z^- = \frac{-iP^+ z^-}{2\sqrt{2}}$; and for $\mu = y$, $\epsilon_{x+-}^y \epsilon_{+}^x p^+ z^- = \frac{P^+ z^-}{2\sqrt{2}}$. The resulting expressions for $\psi_{3;A}^{\perp}(x)$ and f_{ρ}^A are independent of the choice of polarization vector ($h = \pm$) and current component ($\mu = x, y$).

Following the same procedure used for the scalar current and choosing the combination ($h = +, \mu = x$), we obtain the analogs of Eqs. (28) and (29) for $\psi_{3;A}^{\perp}(x)$ and f_{ρ}^A :

$$\begin{aligned} \psi_{3;A}^{\perp}(x) &= \frac{\sqrt{N_c}}{f_{\rho}^A} \int_0^1 dx' \int \frac{d^2 \mathbf{k}_{\perp}}{16\pi^3} \Phi(x', \mathbf{k}_{\perp}) \\ & \times \frac{4\sqrt{2}}{M} \sum_{\lambda_1, \lambda_2} \mathcal{R}'_{\lambda_1 \lambda_2}{}^{11} \left[\frac{\bar{v}_{\lambda_2}(p'_2) \gamma^x \gamma_5 u_{\lambda_1}(p'_1)}{\sqrt{x'_2} \sqrt{x'_1}} \right], \end{aligned} \quad (32)$$

and

$$\begin{aligned} f_{\rho}^A &= \sqrt{N_c} \int_0^1 dx \int_0^x dx' \int \frac{d^2 \mathbf{k}_{\perp}}{16\pi^3} \Phi(x', \mathbf{k}_{\perp}) \\ & \times \frac{4\sqrt{2}}{M} \sum_{\lambda_1, \lambda_2} \mathcal{R}'_{\lambda_1 \lambda_2}{}^{11} \left[\frac{\bar{v}_{\lambda_2}(p'_2) \gamma^x \gamma_5 u_{\lambda_1}(p'_1)}{\sqrt{x'_2} \sqrt{x'_1}} \right]. \end{aligned} \quad (33)$$

¹ In this work, we adopt the convention $\epsilon^{+-xy} = 2$ and use LF metric components $g^{+-} = g^{-+} = 2$

Finally, following the same approach used for f_ρ^S , we obtain

$$f_\rho^A = \sqrt{N_c} \int_0^1 dx \int_0^x dx' \int \frac{d^2 \mathbf{k}_\perp}{16\pi^3} \Phi(x', \mathbf{k}_\perp) \mathcal{O}'_A, \quad (34)$$

where $\mathcal{O}'_A = 2\mathcal{O}'_S$, demonstrating that $f_\rho^A = 2f_\rho^S$ in our model calculation.

Using the QCD equation of motion, it was shown in Ref. [13] that the decay constants f_ρ^A and f_ρ^S can be expressed as linear combinations of f_ρ^\parallel and f_ρ^\perp :

$$\begin{aligned} f_\rho^A &= f_\rho^\parallel - \alpha f_\rho^\perp, \\ f_\rho^S &= f_\rho^\perp - \alpha f_\rho^\parallel. \end{aligned} \quad (35)$$

where $\alpha = 2m/M$ accounts for quark mass corrections. Here, the quark mass m is understood as a constituent quark mass that effectively encodes non-perturbative dynamics such as chiral symmetry breaking and confinement at the hadronic scale. It does not correspond to the QCD scale-dependent running mass. In QCD, the relation $\alpha = 2m/M$, where M is derived from the equation-of-motion relations among light-cone DAs. However, in our BT-based LFQM, the meson is described as a composite $q\bar{q}$ system characterized by an internal invariant mass M_0 , which differs from the physical mass M . To ensure that Eq. (35) is satisfied self-consistently within our model, we should take M as M_0 , yielding $\alpha = 2m/M_0$. This assignment is not arbitrary but essential for obtaining decay constants and DAs that are independent of the choice of current component or polarization state. In contrast, employing a fixed value of $\alpha = 2m/M$ in our model would lead to inconsistencies across different current components. Thus, our consistent treatment of M in the entire computation ensures internal consistency and effectively implements the QCD equation-of-motion constraint within the LF framework.

To verify this consistency explicitly, we demonstrate that Eq. (35) also holds within our LFQM framework. To maintain consistency with the BT construction, the physical mass M in α must be replaced by the invariant mass M_0 , and this replacement must be applied within the integrals. Thus, Eq. (35) becomes, in our LFQM:

$$\begin{aligned} f_\rho^A &= \langle 0 | \frac{\bar{q}\gamma^\mu q}{\mathcal{P}_V^\mu} | P \rangle_{\text{BT}} - \langle 0 | \alpha \frac{\bar{q}\sigma^{\mu\nu} q}{\mathcal{P}_T^{\mu\nu}} | P \rangle_{\text{BT}}, \\ f_\rho^S &= \langle 0 | \frac{\bar{q}\sigma^{\mu\nu} q}{\mathcal{P}_T^{\mu\nu}} | P \rangle_{\text{BT}} - \langle 0 | \alpha \frac{\bar{q}\gamma^\mu q}{\mathcal{P}_V^\mu} | P \rangle_{\text{BT}}. \end{aligned} \quad (36)$$

We define

$$\begin{aligned} \tilde{f}_\rho^\perp &\equiv \langle 0 | \alpha \frac{\bar{q}\sigma^{\mu\nu} q}{\mathcal{P}_T^{\mu\nu}} | P \rangle_{\text{BT}} \\ &= \sqrt{N_c} \int_0^1 dx \int \frac{d^2 \mathbf{k}_\perp}{16\pi^3} \Phi(x, \mathbf{k}_\perp) \\ &\quad \times \frac{2m}{M_0} \frac{1}{\mathcal{P}_T^{\mu\nu}} \sum_{\lambda_1, \lambda_2} \mathcal{R}_{\lambda_1 \lambda_2}^{11} \left[\frac{\bar{v}_{\lambda_2}(p_2)}{\sqrt{x_2}} \sigma^{\mu\nu} \frac{u_{\lambda_1}(p_1)}{\sqrt{x_1}} \right], \end{aligned} \quad (37)$$

TABLE II. Predicted decay constants (in MeV) of the ρ meson obtained from various current operators in our LFQM.

$\rho(1S)$	f_ρ^\parallel	\tilde{f}_ρ^\perp	f_ρ^A	f_ρ^\perp	\tilde{f}_ρ^\parallel	f_ρ^S
$m \neq 0$	215	93	122	173	112	61
$m \rightarrow 0$	190	0	190	95	0	95
Expt. [65]	208 ^a , 216(5) ^b

^a Expt. value for $\Gamma(\tau \rightarrow \rho\nu_\tau)$.

^b Expt. value for $\rho^0 \rightarrow e^+e^-$.

and

$$\begin{aligned} \tilde{f}_\rho^\parallel &\equiv \langle 0 | \alpha \frac{\bar{q}\gamma^\mu q}{\mathcal{P}_V^\mu} | P \rangle_{\text{BT}} \\ &= \sqrt{N_c} \int_0^1 dx \int \frac{d^2 \mathbf{k}_\perp}{16\pi^3} \Phi(x, \mathbf{k}_\perp) \\ &\quad \times \frac{2m}{M_0} \frac{1}{\mathcal{P}_V^\mu} \sum_{\lambda_1, \lambda_2} \mathcal{R}_{\lambda_1 \lambda_2}^{1h} \left[\frac{\bar{v}_{\lambda_2}(p_2)}{\sqrt{x_2}} \gamma^\mu \frac{u_{\lambda_1}(p_1)}{\sqrt{x_1}} \right]. \end{aligned} \quad (38)$$

Note that the factor $\alpha = 2m/M$ is consistently replaced by $2m/M_0$ within the integrals. It is important to emphasize that both \tilde{f}_ρ^\perp and \tilde{f}_ρ^\parallel are independent of current components and polarization vectors within our LFQM, validating the self-consistency of our approach.

The final expressions for \tilde{f}_ρ^\parallel and \tilde{f}_ρ^\perp are given by

$$\tilde{f}_\rho^{\parallel(\perp)} = \sqrt{N_c} \int_0^1 dx \int \frac{d^2 \mathbf{k}_\perp}{16\pi^3} \Phi(x, \mathbf{k}_\perp) \tilde{\mathcal{O}}_{V(T)}, \quad (39)$$

where $\tilde{\mathcal{O}}_{V(T)} = \frac{2m}{M_0} \mathcal{O}_{V(T)}$. We note that in our LFQM, the scale dependence of the decay constants can be approximately incorporated by introducing an ultraviolet cutoff on the transverse momentum: $\int d^2 \mathbf{k}_\perp \rightarrow \int^{|\mathbf{k}_\perp| < \mu} d^2 \mathbf{k}_\perp$. For the nonperturbative Gaussian wave function $\Phi(x, \mathbf{k}_\perp)$ given in Eq. (14), we adopt $\mu_0 \simeq 1$ GeV as the optimal initial scale in our LFQM.

In our numerical analysis of the ρ meson, we use the model parameters $(m, \beta) = (0.25, 0.3194)$ GeV, determined from meson spectrum calculations using a HO confining potential and variational analysis within our standard LFQM framework [29, 34, 35].

The computed ρ meson decay constants (f_ρ^\parallel , f_ρ^\perp , f_ρ^A , f_ρ^S) and $\tilde{f}_\rho^{\parallel(\perp)}$ are summarized in Table II. The values of f_ρ^\parallel and f_ρ^\perp have already been analyzed in Refs. [29, 30, 39]. Our prediction, $f_\rho^\parallel = 215$ MeV, is in excellent agreement with the experimental value of $f_\rho^{\parallel(\text{Expt.})} = 216(5)$ MeV, extracted from $\rho^0 \rightarrow e^+e^-$ [65].

As the main focus of this work, we compute f_ρ^A and f_ρ^S . These decay constants are related to f_ρ^\parallel and f_ρ^\perp via Eq. (35), which follows from the QCD equation of motion [13], and are expressed in our LFQM as $f_\rho^A = f_\rho^\parallel - \tilde{f}_\rho^\perp$, $f_\rho^S = f_\rho^\perp - \tilde{f}_\rho^\parallel$, as shown in Eq. (36). These relations are numerically verified in Table II. Furthermore,

TABLE III. Twist classification of DAs based on the choice of the chirality, current, component, and polarization for vector mesons.

Chirality	Γ	ϵ_h	Twist	DAs
Even	γ^+, γ^\perp	ϵ_0	2	$\phi_{2;V}^\parallel$
	γ^-	ϵ_0	4	$\phi_{4;V}^\parallel$
	γ^\perp, γ^-	ϵ_\pm	3	$\phi_{3;V}^\perp$
	$\gamma^\perp \gamma_5$	ϵ_\pm	3	$\psi_{3;A}^\perp$
Odd	$\sigma^{\perp+}, \sigma^{\perp-}$	ϵ_\pm	2	$\phi_{2;T}^\perp$
	$\sigma^{\perp-}$	ϵ_\pm	4	$\phi_{4;T}^\perp$
	$\sigma^{\perp+}, \sigma^{\perp-}$	ϵ_0	3	$\phi_{3;T}^\parallel$
	$\mathbf{1}$	ϵ_0	3	$\psi_{3;S}^\parallel$

our model satisfies the SU(6) symmetry relation [66], $f_\pi + f_\rho^\parallel = 2f_\rho^\perp$, as demonstrated in Refs. [29, 60]. In the chiral limit (i.e., $m \rightarrow 0$), we also confirm that $f_\rho^A = f_\rho^\parallel$ and $f_\rho^S = f_\rho^\perp$. In this limit, the relation $f_\rho^\parallel = 2f_\rho^\perp$ is obtained within our model.

IV. DISTRIBUTION AMPLITUDES

In this section, we derive the chiral-even DAs from the nonlocal matrix elements of the current operators ($\gamma^\mu, \gamma^\mu \gamma_5$), and the chiral-odd DAs from those of ($\sigma^{\mu\nu}, \mathbf{1}$). The twist classification of these DAs depends on the choice of current components and polarization vectors, as outlined in Ref. [13]. Table III summarizes all possible combinations of current components and polarization vectors that yield nonvanishing matrix elements.

For example, the chiral-even twist-2 DA, $\phi_{2;V}^\parallel(x)$, can be obtained from the γ^+ or γ^\perp components of the vector current, combined with longitudinal polarization ϵ_0 . In contrast, using the minus component γ^- with ϵ_0 leads to the twist-4 DA $\phi_{4;V}^\parallel$. Transverse polarizations ϵ_\pm , combined with γ^- or γ^\perp , yield the twist-3 DA $\phi_{3;V}^\perp$. All DAs satisfy the normalization condition given in Eq. (22). In the following, we present a detailed analysis of both chiral-even and chiral-odd DAs.

A. Chiral-even DA

The chiral-even DAs of a vector meson, associated with the vector current up to twist-4 accuracy, are given

by [16]

$$\begin{aligned}
A_V^\mu(h) &= \langle 0 | \bar{q}(z) \gamma^\mu q(-z) | \rho(P, h) \rangle \\
&= f_\rho^\parallel M \int_0^1 dx e^{-i\zeta P \cdot z} \\
&\quad \times \left[P^\mu \frac{\epsilon_h \cdot z}{P \cdot z} \left(\phi_{2;V}^\parallel(x) + z^2(\dots) \right) \right. \\
&\quad \left. + \left(\epsilon_h^\mu - P^\mu \frac{\epsilon_h \cdot z}{P \cdot z} \right) \phi_{3;V}^\perp(x) - \frac{z^\mu M^2 \epsilon_h \cdot z}{2(P \cdot z)^2} \right. \\
&\quad \left. \times \left(\phi_{4;V}^\parallel(x) + \phi_{2;V}^\parallel(x) - 2\phi_{3;V}^\perp(x) \right) \right], \quad (40)
\end{aligned}$$

where the term proportional to z^2 vanishes under the equal LF time condition, i.e. for a lightlike separation z^μ with $z^2 = z^- z^+ - \mathbf{z}_\perp^2 = 0$, which is realized by setting $z^+ = 0$ and $\mathbf{z}_\perp = 0$. Then, Eq. (40) reduces to

$$\begin{aligned}
A_V^\mu(h) &= f_\rho^\parallel M \int_0^1 dx e^{-i\zeta P \cdot z} \left[P^\mu \frac{\epsilon_h^+}{P^+} \phi_{2;V}^\parallel(x) \right. \\
&\quad \left. + \left(\epsilon_h^\mu - P^\mu \frac{\epsilon_h^+}{P^+} \right) \phi_{3;V}^\perp(x) - \frac{z^\mu M^2 \epsilon_h^+}{z^- P^+ P^+} \right. \\
&\quad \left. \times \left(\phi_{4;V}^\parallel(x) + \phi_{2;V}^\parallel(x) - 2\phi_{3;V}^\perp(x) \right) \right]. \quad (41)
\end{aligned}$$

As summarized in Table III, the twist-2 DA $\phi_{2;V}^\parallel(x)$ can be extracted from either the $\mu = +$ or $\mu = \perp$ component of the vector current with longitudinal polarization ($h = 0$):

$$A_V^{+(\perp)}(0) = f_\rho^\parallel M \epsilon_0^{+(\perp)} \int_0^1 dx e^{-i\zeta P \cdot z} \phi_{2;V}^\parallel(x). \quad (42)$$

The twist-3 DA $\phi_{3;V}^\perp(x)$ can be isolated from either the $\mu = \perp$ or $\mu = -$ component with transverse polarization ($h = \pm 1$):

$$A_V^{\perp(-)}(\pm 1) = f_\rho^\parallel M \epsilon_\pm^{\perp(-)} \int_0^1 dx e^{-i\zeta P \cdot z} \phi_{3;V}^\perp(x). \quad (43)$$

Similarly, the twist-4 DA $\phi_{4;V}^\parallel(x)$ can be extracted from the $\mu = -$ component with longitudinal polarization ($h = 0$) in the $\mathbf{P}_\perp = 0$ frame:

$$A_V^-(0) = f_\rho^\parallel M \epsilon_0^- \int_0^1 dx e^{-i\zeta P \cdot z} \phi_{4;V}^\parallel(x). \quad (44)$$

The explicit forms of the three chiral-even DAs, $\phi_V = \{ \phi_{2;V}^\parallel, \phi_{3;V}^\perp, \phi_{4;V}^\parallel \}$, derived from the vector current, are given by

$$\phi_V(x) = \frac{\sqrt{N_c}}{f_\rho^\parallel} \int \frac{d^2 \mathbf{k}_\perp}{16\pi^3} \Phi(x, \mathbf{k}_\perp) \mathcal{O}_V, \quad (45)$$

where the corresponding operators \mathcal{O}_V , defined for each DA, are

$$\mathcal{O}_V = \{ \mathcal{O}_V^{+(\perp)}(0), \mathcal{O}_V^{\perp(-)}(\pm 1), \mathcal{O}_V^-(0) \}. \quad (46)$$

Their explicit forms are listed in Table I. Notably, as shown in Table I, for the ρ meson, the three operators $\mathcal{O}_V^+(0)$, $\mathcal{O}_V^-(0)$, and $\mathcal{O}_V(0)$ coincide. As a result, the twist-2 DA $\phi_{2;V}^{\parallel}$ and the twist-4 DA $\phi_{4;V}^{\parallel}$ are identical in our model.

Finally, the chiral-even twist-3 DA $\psi_{3;A}^{\perp}(x)$, derived from the nonlocal axial-vector matrix element in Eq. (21), is expressed in Eq. (32) within our LFQM. Applying the BT construction (i.e. $M \rightarrow M_0$) yields the final form:

$$\psi_{3;A}^{\perp}(x) = \frac{\sqrt{N_c}}{f_{\rho}^A} \int_0^x dx' \int \frac{d^2 \mathbf{k}_{\perp}}{16\pi^3} \Phi(x', \mathbf{k}_{\perp}) \mathcal{O}'_A, \quad (47)$$

where $\mathcal{O}'_A = 2\mathcal{O}'_S$ (see Eq. (31)).

B. Chiral-odd DA

The chiral-odd DAs of a vector meson, associated with the tensor current up to twist-4 accuracy, are given by [16]

$$\begin{aligned} A_T^{\mu\nu}(h) &= \langle 0 | \bar{q}(z) \sigma^{\mu\nu} q(-z) | \rho(P, h) \rangle \\ &= i f_{\rho}^{\perp} \int_0^1 dx e^{-i\zeta P \cdot z} \left\{ (\epsilon_h^{\mu} P^{\nu} - \epsilon_h^{\nu} P^{\mu}) \right. \\ &\quad \times [\phi_{2;T}^{\perp}(x) + z^2(\dots)] + (P^{\mu} z^{\nu} - P^{\nu} z^{\mu}) \\ &\quad \times \frac{(\epsilon_h \cdot z) M^2}{(P \cdot z)^2} \left[\phi_{3;T}^{\parallel}(x) - \frac{1}{2} \phi_{2;T}^{\perp}(x) - \frac{1}{2} \phi_{4;T}^{\perp}(x) \right] \\ &\quad \left. + \frac{(\epsilon_h^{\mu} z^{\nu} - \epsilon_h^{\nu} z^{\mu}) M^2}{P \cdot z} \left[\phi_{4;T}^{\perp}(x) - \phi_{2;T}^{\perp}(x) \right] \right\}. \end{aligned} \quad (48)$$

As in Eq. (40), the term proportional to z^2 vanishes under the equal LF time condition, i.e., when $z^+ = z_{\perp} = 0$. This simplifies the expression to

$$\begin{aligned} A_T^{\mu\nu}(h) &= i f_{\rho}^{\perp} \int_0^1 dx e^{-i\zeta P \cdot z} \left\{ (\epsilon_h^{\mu} P^{\nu} - \epsilon_h^{\nu} P^{\mu}) \phi_{2;T}^{\perp}(x) \right. \\ &\quad + \frac{2M^2 \epsilon_h^+ (P^{\mu} z^{\nu} - P^{\nu} z^{\mu})}{z^- P^+ P^+} \\ &\quad \times \left[\phi_{3;T}^{\parallel}(x) - \frac{1}{2} \phi_{2;T}^{\perp}(x) - \frac{1}{2} \phi_{4;T}^{\perp}(x) \right] \\ &\quad \left. + \frac{2M^2 (\epsilon_h^{\mu} z^{\nu} - \epsilon_h^{\nu} z^{\mu})}{P^+ z^-} \left[\phi_{4;T}^{\perp}(x) - \phi_{2;T}^{\perp}(x) \right] \right\}. \end{aligned} \quad (49)$$

As summarized in Table III, the twist-2 DA $\phi_{2;T}^{\perp}(x)$ can be isolated by choosing $\mu\nu = \perp +$ or $+-$ with transverse polarization ($h = \pm 1$), resulting in

$$A_T^{\perp+}(\pm 1) = i f_{\rho}^{\perp} \epsilon_{\pm}^{\perp} P^+ \int_0^1 dx e^{-i\zeta P \cdot z} \phi_{2;T}^{\perp}(x). \quad (50)$$

Similarly, the twist-3 DA $\phi_{3;T}^{\perp}(x)$ can be extracted by taking $\mu\nu = +-$ or $\perp -$ with longitudinal polarization

($h = 0$), yielding

$$A_T^{+ -}(0) = i f_{\rho}^{\perp} \epsilon_0^+ \frac{2M^2}{P^+} \int_0^1 dx e^{-i\zeta P \cdot z} \phi_{3;T}^{\perp}(x). \quad (51)$$

The twist-4 DA $\phi_{4;T}^{\perp}(x)$ is obtained by choosing $\mu\nu = \perp -$ with transverse polarization ($h = \pm 1$), leading to

$$A_T^{\perp-}(\pm 1) = i f_{\rho}^{\perp} \epsilon_{\pm}^{\perp} \frac{2M^2}{P^+} \int_0^1 dx e^{-i\zeta P \cdot z} \phi_{4;T}^{\perp}(x). \quad (52)$$

The three chiral-odd DAs, $\phi_T = \{ \phi_{2;T}^{\perp}, \phi_{3;T}^{\parallel}, \phi_{4;T}^{\perp} \}$, derived from the tensor current, can be expressed as

$$\phi_T(x) = \frac{\sqrt{N_c}}{f_{\rho}^{\perp}} \int \frac{d^2 \mathbf{k}_{\perp}}{16\pi^3} \Phi(x, \mathbf{k}_{\perp}) \mathcal{O}_T, \quad (53)$$

where the corresponding operators \mathcal{O}_T , defined for each DA, are

$$\mathcal{O}_T = \{ \mathcal{O}_T^{\perp+}(\pm 1), \mathcal{O}_T^{\perp-}(0), \mathcal{O}_T^{\perp-}(\pm 1) \}. \quad (54)$$

The explicit forms of these operators are provided in Table I. Similar to the chiral-even case, the two operators $\mathcal{O}_T^{\perp+}(\pm 1)$ and $\mathcal{O}_T^{\perp-}(\pm 1)$ coincide. As a result, the twist-2 DA $\phi_{2;T}^{\perp}$ and the twist-4 DA $\phi_{4;T}^{\perp}$ are identical in our model.

Finally, the chiral-odd twist-3 DA $\psi_{3;S}^{\parallel}(x)$, derived from the nonlocal scalar matrix element in Eq. (21), is expressed in Eq. (28) within our LFQM. Applying the BT construction (i.e. $M \rightarrow M_0$) yields the final form:

$$\psi_{3;S}^{\parallel}(x) = \frac{\sqrt{N_c}}{f_{\rho}^S} \int_0^x dx' \int \frac{d^2 \mathbf{k}_{\perp}}{2(2\pi)^3} \Phi(x', \mathbf{k}_{\perp}) \mathcal{O}'_S. \quad (55)$$

C. Numerical Results

Parts of results for the chiral-even twist-2 and twist-3 DAs of the ρ meson were previously presented in Ref. [30]. In this study, we complete the analysis by including DAs up to twist-4 for both chiral-even and chiral-odd sectors.

Figure 1 shows the chiral-even twist-2 and twist-4 DAs ($\phi_{2;V}^{\parallel}, \phi_{4;V}^{\parallel}$) (upper panel), and the chiral-odd twist-2 and twist-4 DAs ($\phi_{2;T}^{\perp}, \phi_{4;T}^{\perp}$) (lower panel) for the ρ meson. The twist-2 results are also compared with other model calculations [14, 67, 68].

We note that in our LFQM, the twist-2 and twist-4 DAs coincide and follow the asymptotic form $\phi_{\text{asm}}(x) = 6x(1-x)$ in the case of equal quark masses. However, the agreement in this case is fortuitous as the twist-2 and twist-4 DAs indeed differ for mesons with unequal quark masses, reflecting the sensitivity of higher-twist structures to mass asymmetry even within the valence $q\bar{q}$ framework. For the twist-2 DA, the single-humped structure we obtain is consistent with—but slightly narrower than—that from the DSE approach [67] and the HERA-fit [68], while it differs significantly from the double-humped structure predicted by QCD SRs [14]. Our DA is

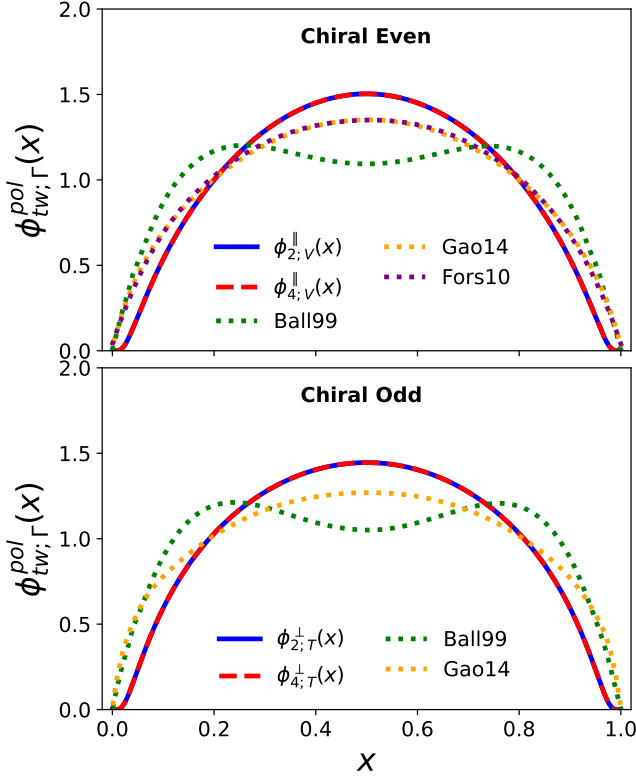


FIG. 1. Chiral-even (upper panel) and chiral-odd (lower panel) twist-2 and twist-4 DAs of the ρ meson from our LFQM, compared with twist-2 DAs from other models, including QCD SRs [14], DSE approach [67], and HERA-fit[68].

more sharply peaked around $x = 1/2$ and more strongly suppressed near the endpoints $x = 0$ and $x = 1$, which may be attributed to the use of a Gaussian radial wave function in our model that naturally favors the central momentum region.

Figure 2 presents the twist-3 DAs of the ρ meson. Our results are also compared with those obtained from QCD SRs [14]. The chiral-even components (upper panel), $\phi_{3;V}^{\parallel}(x)$ and $\psi_{3;A}^{\perp}(x)$, exhibit distinct shapes: $\phi_{3;V}^{\parallel}(x)$ shows a broad double-humped profile, while $\psi_{3;A}^{\perp}(x)$ displays a narrow, single-peaked distribution centered at $x = 1/2$. Compared to the QCD sum rule predictions [14], our $\psi_{3;A}^{\perp}(x)$ is notably more localized, and $\phi_{3;V}^{\parallel}(x)$ differs substantially, lacking the end-point enhancement and double-minimum structure seen in [14]. Interestingly, the shape of our $\phi_{3;V}^{\parallel}(x)$ more closely resembles that of $\psi_{3;A}^{\perp}(x)$ from QCD SRs, though their asymptotic behaviors remain distinct (see Fig. 3).

The chiral-odd twist-3 DAs (lower panel), $\phi_{3;T}^{\perp}(x)$ and $\psi_{3;S}^{\parallel}(x)$, follow similar patterns: $\phi_{3;T}^{\perp}(x)$ shows a more pronounced double-humped structure with deeper suppression at the center, while $\psi_{3;S}^{\parallel}(x)$ has a single central peak, akin to $\psi_{3;A}^{\perp}(x)$. These results again contrast with

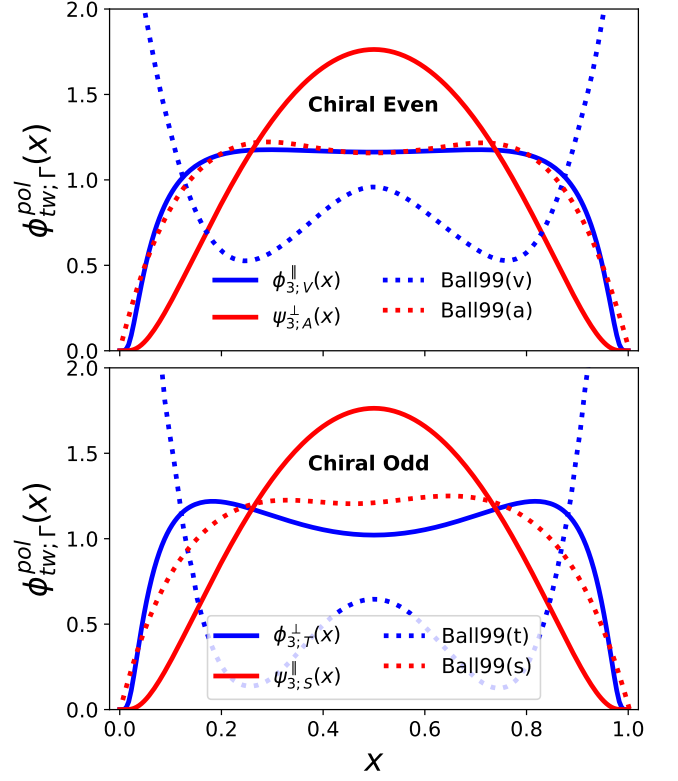


FIG. 2. The chiral-even (upper panel) and chiral-odd (lower panel) twist-3 DAs of the ρ meson from our LFQM, compared with those from QCD SRs [14].

the QCD SRs [14], highlighting the model dependence of twist-3 DAs.

In Fig. 3, we present the chiral-even (upper panel) and chiral-odd (lower panel) DAs of the ρ meson up to twist-4 in the chiral limit ($m \rightarrow 0$). It is evident that our chiral-limit predictions for the chiral-even DAs ($\phi_{2;V}^{\parallel}(x)$, $\phi_{4;V}^{\parallel}(x)$, and $\psi_{3;A}^{\perp}(x)$) coincide and match the asymptotic form $6x(1-x)$. The same holds for the chiral-odd DAs ($\phi_{2;T}^{\perp}(x)$, $\phi_{4;T}^{\perp}(x)$, and $\psi_{3;S}^{\parallel}(x)$) which also coincide and match the asymptotic shape $6x(1-x)$. In contrast, the twist-3 DAs $\phi_{3;V}^{\parallel}(x)$ and $\phi_{3;T}^{\perp}(x)$ exhibit characteristic convex shapes in the chiral limit, consistent with the corresponding asymptotic predictions from QCD SRs [13]. Specifically, $\phi_{3;T}^{\perp}(x)$ matches the asymptotic form $3\xi^2$, where $\xi = 2x - 1$, attaining a value of 3 at the endpoints ($x = 0, 1$) and vanishing at $x = 1/2$, while $\phi_{3;V}^{\parallel}(x)$ follows the asymptotic form $\frac{3}{4}(1 + \xi^2)$, reaching $3/2$ at the endpoints and $3/4$ at $x = 1/2$. These results demonstrate that our LFQM predictions for twist-3 DAs in the chiral limit accurately reproduce the expected asymptotic behavior.

As seen in Fig. 3, the leading- and higher-twist DAs in the chiral limit ($m \rightarrow 0$) approach two types of asymptotic forms—namely, $6x(1-x)$ and $\frac{3}{4}(1 + \xi^2)$ —depending on the twist order. In contrast, in the opposite limit of

TABLE IV. The ξ and Gegenbauer moments up to $n = 6$ for chiral-even and -odd DAs of the ρ meson up to twist 4 compared with other model calculations. The odd moments are vanishing because of the equal mass of the constituent quark.

DA		$\langle \xi^2 \rangle$	$\langle \xi^4 \rangle$	$\langle \xi^6 \rangle$		a_2	a_4	a_6
$\phi_{2;V}^{\parallel}$	Our	0.193	0.078	0.040	Our	-0.020	-0.030	-0.017
	HERA-fit [68]	0.227	0.105	0.062	QCD SRs [13]	0.18(10)
	QCD SRs [69]	0.220(6)	0.103(4)	0.0656(50)	QCD SRs [70]	0.047(58)	-0.057(118)	...
	DSE [67]	0.23	0.11	0.066	QCD SRs [71]	$0.09_{-0.07}^{+0.10}$	0.03(2)	...
	LFH [72]	0.20	0.087	0.048	LFQM [73]	-0.03	-0.09	0.7
	Lattice QCD [74]	0.25(2)(2)	Lattice QCD [75]	0.132(27)
$\phi_{3;V}^{\parallel}$	Our	0.254	0.120	0.069	Our	0.158	-0.018	-0.036
$\psi_{3;A}^{\perp}$	Our	0.153	0.052	0.023	Our	-0.138	-0.023	-0.002
$\phi_{4;V}^{\parallel}$	Our	0.193	0.078	0.040	Our	-0.020	-0.030	-0.017
$\phi_{2;T}^{\perp}$	Our	0.202	0.084	0.044	Our	0.007	-0.032	-0.020
	LFH [72]	0.25	0.13	0.079	QCD SRs [13]	0.2(1)
	DSE [67]	0.25	0.13	0.079	QCD SRs [71]	$0.09_{-0.07}^{+0.10}$	0.03(2)	...
	QCD SRs [76]	0.325(10)	LFQM [73]	0	-0.04	-0.04
	QCD SRs [70]	0.11(1)	0.022(2)	...	Lattice QCD [75]	0.101(22)
	$\phi_{3;T}^{\perp}$	Our	0.278	0.136	0.080	Our	0.228	0.017
$\psi_{3;S}^{\parallel}$	Our	0.153	0.084	0.023	Our	-0.138	-0.023	-0.002
$\phi_{4;T}^{\perp}$	Our	0.202	0.052	0.044	Our	0.007	-0.032	-0.020

the heavy-quark regime ($m \rightarrow \infty$), all DAs converge to a common form proportional to $\delta(x - 1/2)$, independent of twist. This behavior arises from the fact that the LFWF in the heavy-quark limit becomes

$$\phi(x, \mathbf{k}_{\perp}) \propto \delta\left(x - \frac{1}{2}\right) e^{-\frac{\mathbf{k}_{\perp}^2}{2\beta^2}}, \quad (56)$$

indicating a sharp localization of the longitudinal momentum fraction at $x = 1/2$. As a result, the twist-2, -3, and -4 DAs all collapse into a single delta-function-like profile centered at $x = 1/2$, reflecting the suppression of relativistic effects in the heavy-quark limit and the non-relativistic reduction of the internal meson dynamics. Such universal behavior provides a useful theoretical benchmark and differs clearly from the richer structures observed in the chiral and intermediate mass regimes. Further analysis of heavy quarkonia DAs in connection with the non-relativistic limit can be found in Ref. [77].

To facilitate comparison, we compute the ξ -moments up to order $n = 6$, defined as

$$\langle \xi^n \rangle = \int_0^1 dx \xi^n \phi(x), \quad (57)$$

where $\phi(x)$ represents the DA of the ρ meson. These DAs can also be expanded in terms of Gegenbauer polynomials $C_n^{3/2}$ as

$$\phi(x, \mu) = 6x(1-x) \left[1 + \sum_{n=1}^{\infty} a_n(\mu) C_n^{3/2}(\xi) \right], \quad (58)$$

with the coefficients $a_n(\mu)$ are known as Gegenbauer moments. The ξ -moments and Gegenbauer moments are related through specific integral relations [31].

Table IV presents the calculated ξ -moments and the corresponding Gegenbauer moments $a_n(\mu)$ at the scale $\mu = 1$ GeV, along with results from other theoretical approaches for comparison. Our results for the leading-twist DAs show good agreement with those from the light-front holographic (LFH) model [72], QCD SRs [69], and DSE approach [67], but differ from the lattice QCD results [74, 75].

Of special interest, using the soft pion theorem, crossing symmetry, and dispersion relations for the two-pion distribution amplitude (2π DA), the authors in Ref. [78] argued that the second Gegenbauer moment for the leading-twist chiral-even DA $\phi_{2;V}^{\parallel}$ is most likely negative. Their phenomenological analysis predicts the ratio $a_2^{\rho}/a_2^{\pi} = (-1.15 \pm 0.86)(1.0 \pm 0.1) \in [-2.211, -0.261]$. Our model prediction yields $a_2^{\rho} = -0.020$ and $a_2^{\pi} = 0.050$ [29], resulting in $a_2^{\rho}/a_2^{\pi} = -0.400$, thereby satisfying this constraint. While some other models predict a positive sign for a_2 , this discrepancy may stem from the proximity of the DA to its asymptotic form and the strong sensitivity to the choice of model LFWFs. Finally, we note that although leading-twist DAs have been extensively studied, reliable predictions for higher-twist DAs remain limited.

V. CONCLUSION

In this study, we have presented a comprehensive analysis of the ρ meson decay constants and chiral-even and chiral-odd DAs up to twist 4, within the framework of the standard LFQM based on the BT construction [58, 59]. The BT construction provides a consistent framework by

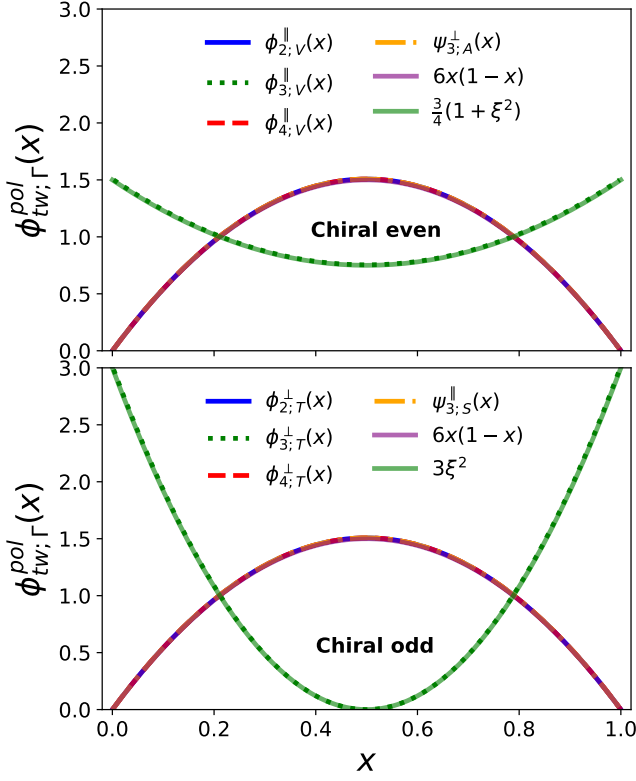


FIG. 3. Chiral-even (upper panel) and chiral-odd (lower panel) DAs of the ρ meson in the chiral limit ($m \rightarrow 0$), calculated in our LFQM. The twist-2 and twist-4, $\psi_{3;A}^{\perp}(x)$, along with $\psi_{3;S}^{\parallel}(x)$ DAs match the asymptotic form $6x(1-x)$. The twist-3 DAs, $\phi_{3;V}^{\parallel}(x)$ and $\phi_{3;T}^{\perp}(x)$, match the asymptotic forms $\frac{3}{4}(1+\xi^2)$ and $3\xi^2$, respectively, as predicted by QCD SRs [14].

incorporating interactions into the Casimir mass operator, ensuring compliance with the Poincaré group symmetry, and allowing the description of mesons as bound states of non-interacting quarks and antiquarks.

We note that, within the BT construction adopted in our LFQM, the total LF momentum operator is designed to satisfy the Poincaré algebra, ensuring Lorentz symmetry at the level of the wave function. Consequently, quantities such as decay constants and DAs extracted from different current components or polarization states are expected to agree by construction. Our explicit calculations thus serve as a numerical confirmation of this self-consistency, verifying that our implementation faithfully preserves the anticipated symmetry properties.

For the ρ meson, which exhibits both longitudinal and transverse polarizations, we have computed all relevant decay constants ($f_{\rho}^{\parallel}, f_{\rho}^{\perp}, f_{\rho}^A, f_{\rho}^S$) associated with various current operators $\Gamma = (\gamma^{\mu}, \sigma^{\mu\nu}, \gamma^{\mu}\gamma_5, \mathbf{1})$. As these de-

cay constants are physical observables, their theoretical predictions must be entirely independent of the computational convenience of choosing current components, polarization states and reference frames. For the first time, we have demonstrated this self-consistency within the LFQM in the computation of these decay constants.

The extraction of decay constants from axial-vector and scalar currents posed a particularly nontrivial challenge due to the mixing between f_{ρ}^{\parallel} and f_{ρ}^{\perp} arising from quark mass corrections, expressed as $f_{\rho}^A = f_{\rho}^{\parallel} - \alpha f_{\rho}^{\perp}$ and $f_{\rho}^S = f_{\rho}^{\perp} - \alpha f_{\rho}^{\parallel}$, with $\alpha = 2m/M$. By applying the BT construction consistently, we resolved these mixings without encountering singularities, ensuring self-consistent robust and reliable results. This work complements and extends our earlier studies [39, 60], further confirming the applicability of the BT construction beyond two-point functions and demonstrating its utility in three-point and higher-order processes [46, 61].

Furthermore, we have predicted the full set of chiral-even DAs ($\phi_{2;V}^{\parallel}, \phi_{3;V}^{\parallel}, \psi_{3;A}^{\perp}, \phi_{4;V}^{\parallel}$) and chiral-odd DAs ($\phi_{2;T}^{\perp}, \phi_{3;T}^{\perp}, \psi_{3;S}^{\parallel}, \phi_{4;T}^{\perp}$) beyond the leading twist. These eight DAs reveal rich structural information about the ρ meson. Notably, in the chiral limit ($m \rightarrow 0$), our predicted DAs are consistent with those from QCD SRs [13], lending further credibility to our LFQM.

Despite the complexity of the ρ meson, the methodology and results demonstrated here can be readily extended to other mesons and observables. Future lattice QCD simulations may serve as valuable benchmarks for validating these predictions.

In conclusion, this work presents a self-consistent and process-independent implementation of the LFQM based on the BT framework. It offers a significant step forward to providing a reliable tool for the study of hadron structure and spectroscopy.

ACKNOWLEDGMENT

A. J. A acknowledges the hospitality of Kyungpook National University during his stay, which facilitated the completion of this work. We thank Kazuhiro Tanaka for useful communications. The work of H.-M. C. was supported by the National Research Foundation of Korea(NRF) under Grant No. RS-2023-NR076506. The work of C.-R.J. was supported in part by the U.S. Department of Energy (Grant No. DE-FG02-03ER41260). The National Energy Research Scientific Computing Center (NERSC) supported by the Office of Science of the U.S. Department of Energy under Contract No. DE-AC02-05CH11231 is also acknowledged.

[1] G. P. Lepage and S. J. Brodsky, Exclusive Processes in Perturbative Quantum Chromodynamics, *Phys. Rev. D*

- [2] A. V. Efremov and A. V. Radyushkin, Factorization and asymptotic behaviour of pion form factor in QCD, *Phys. Lett. B* **94**, 245 (1980).
- [3] V. L. Chernyak and A. R. Zhitnitsky, Asymptotic Behavior of Exclusive Processes in QCD, *Phys. Rept.* **112**, 173 (1984).
- [4] T. Abe *et al.* (Belle-II), Belle II Technical Design Report, (2010).
- [5] R. Aaij *et al.* (LHCb), Implications of LHCb measurements and future prospects, *Eur. Phys. J. C* **73**, 2373 (2013).
- [6] J. Dudek *et al.*, Physics Opportunities with the 12 GeV Upgrade at Jefferson Lab, *Eur. Phys. J. A* **48**, 187 (2012).
- [7] A. Accardi, J. L. Albacete, M. Anselmino, N. Armesto, E. C. Aschenauer, A. Bacchetta, D. Boer, W. K. Brooks, T. Burton, N. B. Chang, *et al.*, Electron Ion Collider: The Next QCD Frontier: Understanding the glue that binds us all, *Eur. Phys. J. A* **52**, 268 (2016).
- [8] R. Abdul Khalek *et al.*, Science Requirements and Detector Concepts for the Electron-Ion Collider: EIC Yellow Report, *Nucl. Phys. A* **1026**, 122447 (2022).
- [9] V. M. Braun, Higher Twists, *EPJ Web Conf.* **274**, 01012 (2022).
- [10] P. Kroll and K. Passek-Kumerički, Twist-3 contributions to wide-angle photoproduction of pions, *Phys. Rev. D* **97**, 074023 (2018).
- [11] M. Beneke, G. Buchalla, M. Neubert, and C. T. Sachrajda, QCD factorization in $B \rightarrow \pi K, \pi\pi$ decays and extraction of Wolfenstein parameters, *Nucl. Phys. B* **606**, 245 (2001).
- [12] H. Beppu, Y. Koike, K. Tanaka, and S. Yoshida, Single Transverse-Spin Asymmetry in Large P_T Open Charm Production at an Electron-Ion Collider, *Phys. Rev. D* **85**, 114026 (2012).
- [13] P. Ball, V. M. Braun, Y. Koike, and K. Tanaka, Higher twist distribution amplitudes of vector mesons in QCD: Formalism and twist - three distributions, *Nucl. Phys. B* **529**, 323 (1998).
- [14] P. Ball and V. M. Braun, Higher twist distribution amplitudes of vector mesons in QCD: Twist - 4 distributions and meson mass corrections, *Nucl. Phys. B* **543**, 201 (1999).
- [15] P. Ball, V. M. Braun, and A. Lenz, Higher-twist distribution amplitudes of the K meson in QCD, *JHEP* **05**, 004.
- [16] P. Ball, V. M. Braun, and A. Lenz, Twist-4 distribution amplitudes of the K^* and ϕ mesons in QCD, *JHEP* **08**, 090.
- [17] T. Huang, X. H. Wu, and M. Z. Zhou, Twist-3 distribution amplitude of the pion in QCD sum rules, *Phys. Rev. D* **70**, 014013 (2004).
- [18] S. V. Mikhailov, A. V. Pimikov, and N. G. Stefanis, End-point behavior of the pion distribution amplitude in QCD sum rules with nonlocal condensates, *Phys. Rev. D* **82**, 054020 (2010).
- [19] D.-D. Hu, X.-G. Wu, L. Zeng, H.-B. Fu, and T. Zhong, Improved light-cone harmonic oscillator model for the ϕ -meson longitudinal leading-twist light-cone distribution amplitude and its effects to $D_s^+ \rightarrow \phi \ell^+ \nu_\ell$, *Phys. Rev. D* **110**, 056017 (2024).
- [20] S. S. Agaev, Impact of the higher twist effects on the $\gamma\gamma^* \rightarrow \pi^0$ transition form factor, *Phys. Rev. D* **72**, 114010 (2005), erratum: *Phys. Rev. D* **73**, 059902 (2006).
- [21] V. Y. Petrov, M. V. Polyakov, R. Ruskov, C. Weiss, and K. Goeke, Pion and photon light-cone wave-functions from the instanton vacuum, *Phys. Rev. D* **59**, 114018 (1999).
- [22] S. I. Nam and H.-C. Kim, Twist-3 pion and kaon distribution amplitudes from the instanton vacuum with flavor SU(3) symmetry breaking, *Phys. Rev. D* **74**, 096007 (2006).
- [23] W.-Y. Liu, E. Shuryak, and I. Zahed, Hadronic structure on the light front. VIII. Light scalar and vector mesons, *Phys. Rev. D* **109**, 074029 (2024).
- [24] E. R. Arriola and W. Broniowski, Pion light-cone wave-function and pion distribution amplitude in the Nambu–Jona-Lasinio model, *Phys. Rev. D* **66**, 094016 (2002).
- [25] M. Praszalowicz and A. Rostworowski, Pion light cone wave-function in the nonlocal NJL model, *Phys. Rev. D* **64**, 074003 (2001).
- [26] L. Chang, C. D. Roberts, and S. M. Schmidt, Light front distribution of the chiral condensate, *Phys. Lett. B* **727**, 255 (2013).
- [27] C. Shi, C. Chen, L. Chang, C. D. Roberts, S. M. Schmidt, and H.-S. Zong, Kaon and pion parton distribution amplitudes to twist three, *Phys. Rev. D* **92**, 014035 (2015).
- [28] C.-W. Hwang, Analyses of decay constants and light-cone distribution amplitudes for s -wave heavy meson, *Phys. Rev. D* **81**, 114024 (2010).
- [29] H.-M. Choi and C.-R. Ji, Distribution amplitudes and decay constants for (π, K, ρ, K^*) mesons in the light-front quark model, *Phys. Rev. D* **75**, 034019 (2007).
- [30] H. M. Choi and C. R. Ji, Self-consistent covariant description of vector meson decay constants and chirality-even quark-antiquark distribution amplitudes up to twist-3 in the light-front quark model, *Phys. Rev. D* **89**, 033011 (2014).
- [31] H. M. Choi and C. R. Ji, Consistency of the light-front quark model with chiral symmetry in the pseudoscalar meson analysis, *Phys. Rev. D* **91**, 014018 (2015).
- [32] H. M. Choi and C. R. Ji, Two-particle twist-3 distribution amplitudes of the pion and kaon in the light-front quark model, *Phys. Rev. D* **95**, 056002 (2017).
- [33] S. J. Brodsky, H.-C. Pauli, and S. S. Pinsky, Quantum chromodynamics and other field theories on the light cone, *Phys. Rept.* **301**, 299 (1998).
- [34] H.-M. Choi and C.-R. Ji, Mixing angles and electromagnetic properties of ground state pseudoscalar and vector meson nonets in the light-cone quark model, *Phys. Rev. D* **59**, 074015 (1999).
- [35] H.-M. Choi and C.-R. Ji, Light-front quark model analysis of exclusive $0^- \rightarrow 0^-$ semileptonic heavy meson decays, *Phys. Lett. B* **460**, 461 (1999).
- [36] H.-M. Choi, C.-R. Ji, Z. Li, and H.-Y. Ryu, Variational analysis of mass spectra and decay constants for ground state pseudoscalar and vector mesons in the light-front quark model, *Phys. Rev. C* **92**, 055203 (2015).
- [37] N. Dhiman, H. Dahiya, C.-R. Ji, and H.-M. Choi, Twist-2 pseudoscalar and vector meson distribution amplitudes in light-front quark model with exponential-type confining potential, *Phys. Rev. D* **100**, 014026 (2019).
- [38] A. J. Arifi, H. M. Choi, C. R. Ji, and Y. Oh, Mixing effects on 1S and 2S state heavy mesons in the light-front quark model, *Phys. Rev. D* **106**, 014009 (2022).
- [39] A. J. Arifi, H.-M. Choi, C.-R. Ji, and Y. Oh, Independence of current components, polarization vectors, and

- reference frames in the light-front quark model analysis of meson decay constants, *Phys. Rev. D* **107**, 053003 (2023).
- [40] H.-Y. Cheng, C.-Y. Cheung, and C.-W. Hwang, Mesonic form-factors and the Isgur-Wise function on the light front, *Phys. Rev. D* **55**, 1559 (1997).
- [41] W. Jaus, Semileptonic decays of B and D mesons in the light-front formalism, *Phys. Rev. D* **41**, 3394 (1990).
- [42] W. Jaus, Relativistic constituent-quark model of electroweak properties of light mesons, *Phys. Rev. D* **44**, 2851 (1991).
- [43] H.-M. Choi, Self-consistent light-front quark model analysis of $B \rightarrow Dlv_l$ transition form factors, *Phys. Rev. D* **103**, 073004 (2021).
- [44] H.-M. Choi, Current-component independent transition form factors for semileptonic and rare $D \rightarrow \pi(K)$ decays in the light-front quark model, *Adv. High Energy Phys.* **2021**, 4277321 (2021).
- [45] A. J. Arifi, L. Happ, S. Ohno, and M. Oka, Structure of heavy mesons in the light-front quark model, *Phys. Rev. D* **110**, 014020 (2024).
- [46] M. Ridwan, A. J. Arifi, and T. Mart, Self-consistent M1 radiative transitions of excited B_c and heavy quarkonia with different polarizations in the light-front quark model, *Phys. Rev. D* **111**, 016011 (2025).
- [47] B. Pandya, B. Gurjar, D. Chakrabarti, H.-M. Choi, and C.-R. Ji, Mixing effects on spectroscopy and partonic observables of heavy mesons with logarithmic confining potential in a light-front quark model, *Phys. Rev. D* **110**, 094021 (2024).
- [48] B. D. Keister, Rotational covariance and light-front current matrix elements, *Phys. Rev. D* **49**, 1500 (1994).
- [49] H.-M. Choi and C.-R. Ji, Nonvanishing zero modes in the light-front current, *Phys. Rev. D* **58**, 071901(R) (1998).
- [50] S. J. Brodsky and D. S. Hwang, Exact light-cone wavefunction representation of matrix elements of electroweak currents, *Nucl. Phys. B* **543**, 239 (1999).
- [51] W. Jaus, Covariant analysis of the light-front quark model, *Phys. Rev. D* **60**, 054026 (1999).
- [52] J. Carbonell, B. Desplanques, V. A. Karmanov, and J. F. Mathiot, Explicitly covariant light-front dynamics and relativistic few-body systems, *Phys. Rep.* **300**, 215 (1998).
- [53] J. de Melo, T. Frederico, E. Pace, and G. Salmè, Pair term in the electromagnetic current within the front-form dynamics: spin-0 case, *Nucl. Phys. A* **707**, 399 (2002).
- [54] B. L. G. Bakker, H.-M. Choi, and C.-R. Ji, Regularizing the divergent structure of light-front currents, *Phys. Rev. D* **63**, 074014 (2001).
- [55] B. L. G. Bakker, H.-M. Choi, and C.-R. Ji, The vector meson form factor analysis in light-front dynamics, *Phys. Rev. D* **65**, 116001 (2002).
- [56] J. P. C. B. de Melo, H. W. L. Naus, and T. Frederico, Pion electromagnetic current in the light cone formalism, *Phys. Rev. C* **59**, 2278 (1999).
- [57] H. J. Melosh, Quarks: Currents and constituents, *Phys. Rev. D* **9**, 1095 (1988).
- [58] B. Bakamjian and L. H. Thomas, Relativistic particle dynamics. II, *Phys. Rev.* **92**, 1300 (1953).
- [59] B. D. Keister and W. N. Polyzou, Relativistic Hamiltonian dynamics in nuclear and particle physics, *Adv. Nucl. Phys.* **20**, 225 (1991).
- [60] A. J. Arifi, H.-M. Choi, and C.-R. Ji, Pseudoscalar meson decay constants and distribution amplitudes up to the twist-4 in the light-front quark model, *Phys. Rev. D* **108**, 013006 (2023).
- [61] H.-M. Choi and C.-R. Ji, Consistency of the pion form factor and unpolarized transverse momentum dependent parton distributions beyond leading twist in the light-front quark model, *Phys. Rev. D* **110**, 014006 (2024).
- [62] F. Cardarelli, I. L. Grach, I. M. Narodetsky, G. Salme, and S. Simula, Electromagnetic form-factors of the rho meson in a light front constituent quark model, *Phys. Lett. B* **349**, 393 (1995).
- [63] H.-Y. Cheng, C.-K. Chua, and C.-W. Hwang, Covariant light-front approach for s -wave and p -wave mesons: Its application to decay constants and form factors, *Phys. Rev. D* **69**, 074025 (2004).
- [64] H. Y. Cheng and C. K. Chua, Light-front approach for Pentaquark strong decays, *JHEP* **11**, 072.
- [65] S. Navas *et al.* (Particle Data Group), Review of particle physics, *Phys. Rev. D* **110**, 030001 (2024).
- [66] H. Leutwyler, Mesons in terms of quarks on a null plane, *Nuclear Physics B* **76**, 413 (1974).
- [67] F. Gao, L. Chang, Y.-X. Liu, C. D. Roberts, and S. M. Schmidt, Parton distribution amplitudes of light vector mesons, *Phys. Rev. D* **90**, 014011 (2014).
- [68] J. R. Forshaw and R. Sandapen, Extracting the rho meson wavefunction from HERA data, *JHEP* **11**, 037.
- [69] T. Zhong, Y.-H. Dai, and H.-B. Fu, ρ -meson longitudinal leading-twist distribution amplitude revisited and the $D \rightarrow \rho$ semileptonic decay, *Chin. Phys. C* **48**, 063108 (2024).
- [70] A. V. Pimikov, S. V. Mikhailov, and N. G. Stefanis, Rho meson distribution amplitudes from QCD sum rules with nonlocal condensates, *Few Body Syst.* **55**, 401 (2014).
- [71] P. Ball and R. Zwicky, $B_{d,s} \rightarrow \rho, \omega, K^*, \phi$ decay form-factors from light-cone sum rules revisited, *Phys. Rev. D* **71**, 014029 (2005).
- [72] B. Gurjar, C. Mondal, and S. Kaur, ρ -meson spectroscopy and diffractive production using the holographic light-front Schrödinger equation and the 't Hooft equation, *Phys. Rev. D* **109**, 094017 (2024).
- [73] C. R. Ji, P. L. Chung, and S. R. Cotanch, Light cone quark model axial vector meson wave function, *Phys. Rev. D* **45**, 4214 (1992).
- [74] R. Arthur, P. A. Boyle, D. Brommel, M. A. Donnellan, J. M. Flynn, A. Juttner, T. D. Rae, and C. T. C. Sachrajda, Lattice Results for Low Moments of Light Meson Distribution Amplitudes, *Phys. Rev. D* **83**, 074505 (2011).
- [75] V. M. Braun *et al.*, The ρ -meson light-cone distribution amplitudes from lattice QCD, *JHEP* **04**, 082.
- [76] A. P. Bakulev and S. V. Mikhailov, The rho meson and related meson wave functions in QCD sum rules with nonlocal condensates, *Phys. Lett. B* **436**, 351 (1998).
- [77] H.-M. Choi and C.-R. Ji, Perturbative qcd analysis of exclusive $j/\psi + \eta_c$ production in e^+e^- annihilation, *Phys. Rev. D* **76**, 094010 (2007).
- [78] M. V. Polyakov and H.-D. Son, Second Gegenbauer moment of a ρ -meson distribution amplitude, *Phys. Rev. D* **102**, 114005 (2020).